Regular Article

Impact of Optical Crosstalk on OIRS-Assisted HAP-Based Multiuser FSO Systems over Turbulence Channels

Bach Q. Tran[1,2], Thang V. Nguyen[1], Hien T. T. Pham[1], Ngoc T. Dang[1]

[1] Wireless System and Application Lab., Posts and Telecommunications Institute of Technology, Hanoi, Vietnam

[2] Faculty of Electronics and Computer Engineering, University of Economics - Technology for Industries, Hanoi, Vietnam

Correspondence: Ngoc T. Dang ngocdt@ptit.edu.vn

Communication: received 25 August 2025, revised 06 November 2025, accepted 13 November 2025

Online publication: 18 November 2025, Digital Object Identifier: 10.21553/rev-jec.417

Abstract– **Free-space optical communication (FSO) utilizes laser beams to transmit data through the atmosphere. However, FSO faces significant challenges, including the strict requirement for line-of-sight (LoS) communication and terrestrial obstacles, which limit its scalability to connect multiple users in diverse environments. To address these limitations and enable reliable multi-user connectivity, the integration of high-altitude platforms (HAP) and optical intelligent reflecting surfaces (OIRS) has emerged as a critical solution. To serve multiple users simultaneously, an OIRS is equipped at the HAP to dynamically control the reflected beam from a ground station to the terminals. This study analyzes the proposed FSO system performance through the outage probability. During the analysis, practically influencing factors such as optical crosstalk, i.e., interference between OIRS regions, and atmospheric turbulence, are considered. The numerical results show the feasibility of deploying OIRS on HAP to support multiuser FSO systems. In addition, properly designing the OIRS coverage could improve the overall performance of the multiuser FSO system.**

Keywords– **Intelligent reconfigurable surface (IRS), Free-space optical (FSO), High-altitude platform (HAP), Optical crosstalk, Spatial division multiple access (SDMA).**

1 Introduction

With the ever-growing demand for high-capacity and low-latency data transmission in next-generation wireless networks, especially within sixth-generation (6G) systems, free-space optical (FSO) communication has emerged as a viable alternative to enhance or replace traditional radio frequency (RF) systems [1, 2]. In contrast to RF, which has spectrum limitations, significant interference, and security risks, FSO utilizes highly directed laser beams to provide vast bandwidth, robust interference resistance, and enhanced communication security [3, 4]. However, despite their considerable benefits, FSO systems are fundamentally restricted by the stringent necessity for line-of-sight (LoS) transmission and are particularly susceptible to terrestrial obstructions, atmospheric conditions, or dynamic entities, which significantly hamper their scalability in multiuser contexts [5]. To address these challenges, high-altitude platforms (HAPs) have garnered considerable attention due to their wide coverage, flexible deployment capabilities, and lower costs compared to satellite-based systems. Integrating FSO with HAPs enables alleviation of LoS obstructions and improves reliable connections in physically demanding places, such as mountain regions, distant islands, or emergency zones where terrestrial infrastructure is difficult to establish [6, 7].

In addition, supporting multiple users simultaneously requires further enhancement of the flexibility of the FSO system. Optical intelligent reflecting surfaces (OIRSs) have recently emerged as a viable option, allowing dynamic regulation of optical beam reflection from the HAP to the terrestrial terminals [8]. Utilizing OIRS enables the successful establishment of multiuser connections while expanding the coverage area. However, a significant concern emerges in OIRS-assisted systems: optical crosstalk [9–11]. Limited phase control and the constrained dimensions of OIRS components may cause reflected beams to overlap or infiltrate adjacent areas, resulting in mutual interference among users. This phenomenon reduces the signal-to-noise ratio (SNR), increases the bit error rate (BER), and eventually compromises system dependability.

In recent years, numerous studies have focused on the terrestrial/non-terrestrial FSO system assisted by RIS [9–15]. In [12], the authors investigated the physical effects of this system; the turbulence-induced fading is modeled as a Gamma-Gamma distribution, and the designated misalignment loss is modeled as a Hoyt distribution; these channel coefficients contribute to performance evaluation in terms of ergodic capacity. In a similar work [13], Malik *et al.* analyzed the impact of atmospheric turbulence together with phase shift errors which arise from the existence of reflective components in the IRS and influence the reflected beam. In [14], the authors statistically characterized the cumulative impacts of the three impairments: atmospheric turbulence, angle of arrival variability of the UAV, and geometric and misalignment loss resulting from changes

in the transmitter, OIRS, and the UAV's location and orientation. Besides, a channel model for an IRS-aided FSO system, based on the Huygens-Fresnel principle, was developed in [15] to facilitate the sharing of the optical IRS among many FSO links. In [9], the control mode, power efficiency, and beam splitting of point-to-multipoint FSO systems were assessed based on the physical models of two types: micro-mirror array and phased array. Nonetheless, the aforementioned studies predominantly focused on the use of a singular source, often utilized for broadcasting transmission methods. In the report of [10], Haibo Wang *et al.* examined the impact of beam jitter, IRS jitter, and obstruction probability on the bit error rate (BER) of a comparable system, demonstrating that the performance of the IRS-assisted multi-branch system surpassed that of the single-branch systems. In addition, the authors developed an IRS-assisted multiuser FSO system utilizing numerous sources, which can accommodate various applications through the use of space division multiple access (SDMA) techniques. However, analysis of the system was limited by focusing solely on the impact of interference optical power, neglecting the critical factor of atmospheric turbulence in the FSO channel model, which is essential for both terrestrial and aerial FSO systems, and was not examined in the prior study.

This study makes significant contributions to the design and analysis of OIRS-aided FSO systems, particularly in the context of HAP-based deployments that serve multiple users, as shown in Figure 1. The key contributions are outlined as follows

- **Deployment of OIRS on HAP for Multiuser Support:** We propose and implement an innovative OIRS-aided FSO system mounted on a HAP to serve multiple users simultaneously. By leveraging the flexible beam control capabilities of OIRS, the system enhances connectivity and coverage, particularly in challenging environments such as remote or obstacle-rich areas, enabling robust multiuser communication with improved reliability.
- **Analyzing the Impact of Optical Crosstalk and Atmospheric Turbulence with the F-Channel Model:** The study comprehensively analyzes the impact of optical crosstalk between OIRS elements and atmospheric turbulence on system performance. Unlike traditional channel models such as log-normal or gamma-gamma distributions, we adopt the Fisher-Snedecor F distribution to model turbulence-induced fading, which offers superior correlation with empirical data. A closed-form expression for the composite channel model is derived, which incorporates propagation loss, turbulence-induced fading, and pointing misalignment, providing a precise framework for performance evaluation. The developed theoretical composited channel is verified by Monte-Carlo simulation to confirm the accuracy.
- **System Performance Evaluation and Practical Deployment Recommendations:** We rigorously evaluate system performance through key metrics, focusing on outage probability. The analysis highlights the detrimental effects of crosstalk and turbulence, particularly in high-density OIRS configurations. To facilitate practical deployment, we propose optimized system parameters, including OIRS element separation distances (7 cm, 15 cm, and 25 cm for weak, moderate, and strong turbulence conditions, respectively), to minimize crosstalk and ensure channel independence, thereby enhancing system reliability and ease of implementation in real-world applications.

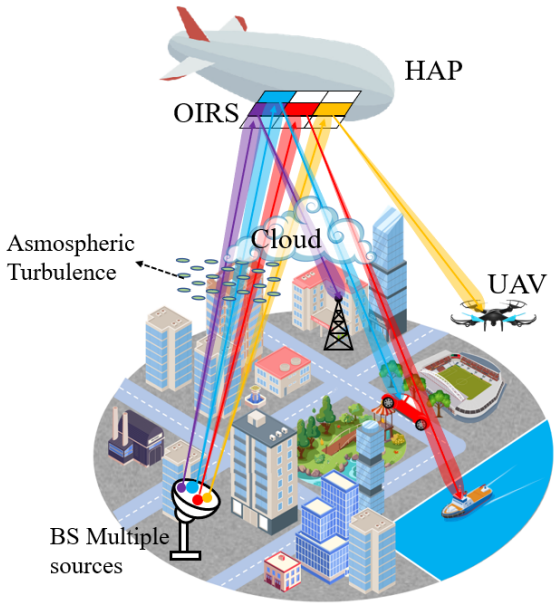

Figure 1. OIRS-aided multiuser FSO system scenario.

The remainder of the paper is structured as follows. Section 2 addresses the atmospheric channel model, which accounts for propagation loss and fading generated by atmospheric turbulence, and presents the integrated atmospheric channel and OIRS vibration model. The performance of the system is analyzed in Section 4. Section 5 shows the numerical results. Finally, Section 6 concludes the paper.

2 System Model

2.1 System Description

We assume that the base station is equipped with n laser transmitters, each designated for a distinct user. The OIRS needs to be divided into n zones to autonomously regulate the beams from n transmitters. The transmitter i transmits the optical signal to region i of the OIRS. The optical signal is then reflected to the user i. The signal received by the user i, represented as y_i, can be expressed as follows [10]

$$y_i = t_i + g_i, \tag{1}$$

where t_i denotes the transmitted signal that goes through the i-th fading channel, specifically from the

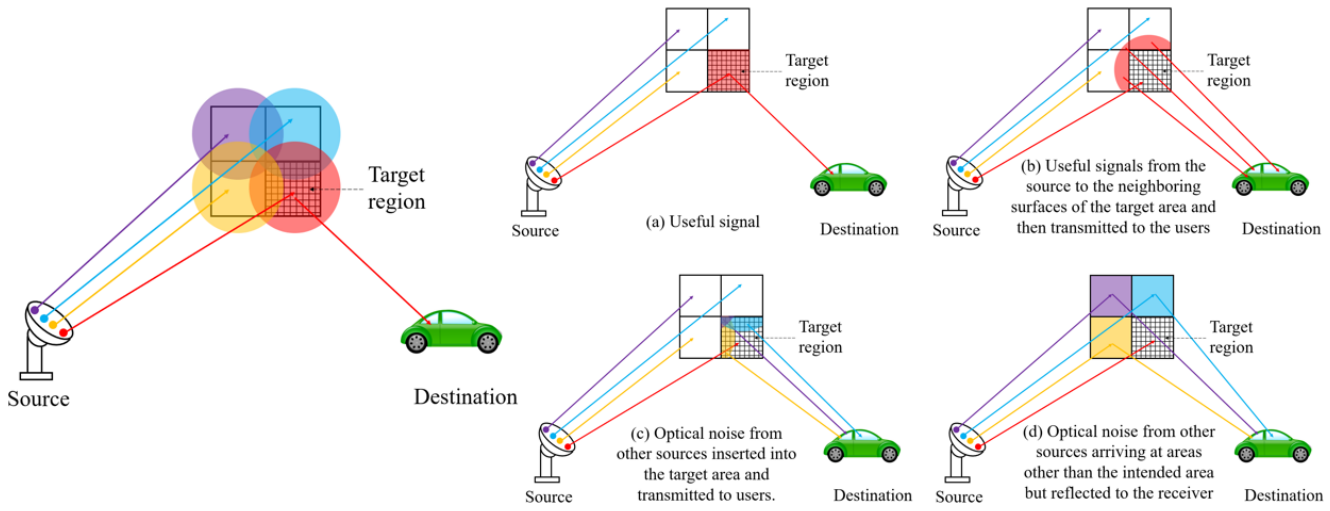

Figure 2. System model of OIRS-aided multiuser FSO with crosstalk optical power illustration.

i-th transmitter to the i-th OIRS element to the i-th user. g_i denotes the Gaussian white noise at the receiver, characterized by a mean of zero and a variance of $\sigma_{g_i}^2$. Presuming the transmitter comprises four optical beams, OIRS is divided into four elements, with four intended consumers located at distinct places. As illustrated in Figure 2, the optical signal is received in the user plane, comprising both desired and crosstalk signals. The desired signal comprises the (1) signal from the i-th transmitter to the i-th OIRS element directed towards the i-th users (refer to Equation (3a) and Figure 2(a)), and the signal from the i-th transmitter to other OIRS elements, excluding the i-th region directed towards the i-th users (refer to Equation (3b) and Figure 2(b)). The extraneous signal comprises (1) interference from additional transmitters, denoting the i-th OIRS element (refer to Equation (3c) and Figure 2(c)), and (2) interference from other transmitters, signifying all OIRS elements excluding the i-th region (refer to Equation (3d) and Figure 2(d)). The signal of the i-th user in (1) can be reformulated as

$$t_i = s_i^{(a)} + s_i^{(b)} + s_i^{(c)} + s_i^{(d)}, \tag{2}$$

where each component of 2 can be expressed as

$$s_i^{(a)} = h_{s_i o_i} h_{o_i u_i} s_i, \tag{3a}$$

$$s_i^{(b)} = \sum_{j=1, j\neq i}^{N} h_{s_i o_j} h_{o_j u_i} s_i, \tag{3b}$$

$$s_i^{(c)} = \sum_{j=1, j\neq i}^{N} \sum_{p=1, p\neq i}^{N} h_{s_j o_p} h_{o_p u_i} s_j, \tag{3c}$$

$$s_i^{(d)} = \sum_{j=1, j\neq i}^{N} h_{s_j o_i} h_{o_i u_i} s_j, \tag{3d}$$

where s_i represents the transmitted signal and s_j denotes the interference source. $h_{s_i o_i}$ and $h_{o_i u_i}$ represent the channel coefficients for the source-to-OIRS channel and the OIRS-to-users channel, respectively.

We utilize an OIRS that is segmented into four square arrays of identical size. This configuration ensures that each primary zone is surrounded by three adjacent portions, as illustrated in Figure 2. Given the proximity of the areas within the OIRS and the generally modest dimensions of the OIRS region, it is likely that the i-th region may receive signals from other sources. The main source of noise signals in the main area originates from these three surrounding segments. The optical power of the beams focused on the i-th region (the primary region) and conveyed to other locations can be formulated as

$$P_{o_i} = P_i \exp\left(-\frac{d_i^2}{2\omega_L^2}\right), \tag{4}$$

where P_i indicates the incident light power of the i-th region, d_i refers to the side length of the i-th region, and ω_z denotes the beam waist radius of the incident beam. Similarly, the overflow optical powers corresponding to the i-th area can be represented as

$$P_{i_{n_t}} = \sum_{m\in M_i} \frac{1}{8} P_m \exp\left(\frac{-d_m^2}{2\omega_z^2}\right), \tag{5}$$

where n_t represents the count of adjacent regions connected to the main area under investigation. The set M_i denotes the adjacent areas associated with the i-th region, while P_m reflects the surplus power of those adjacent regions. This study investigates the overflow power in the regions, assuming that it is uniform. This assumption is based on an estimation formula developed from the region partitioning method, facilitating a rapid assessment of the intensity of the noise signal in adjacent areas [10].

3 Channel Model

In OIRS-assisted multiuser HAP-based FSO systems, the transmission of an optical signal is mainly affected

by three critical factors: propagation loss, fading due to atmospheric turbulence, and fading resulting from pointing misalignment. As a result, the overall channel coefficient h_i can be formulated as follows

$$h_i = h_{a_i} h_{p_i} h_{l_i}, \tag{6}$$

where h_{l_i} represents the propagation loss, which depends on both the transmission distance and atmospheric conditions, meanwhile h_{p_i} signifies the power loss attributed to the misalignment of the transceiver and is represented by a stochastic variable. Ultimately, h_{a_i} constitutes a random variable that characterizes the fading induced by intensity variations of the optical beam that passes through the atmospheric turbulence channel.

3.1 Propagation Loss

In free space, the optical signal experiences attenuation during its propagation in the atmospheric channel due to absorption and scattering. The channel loss coefficient can be articulated in accordance with the Beer-Lambert law as

$$h_{l_i} = \exp(-\alpha_{l_i} L), \tag{7}$$

where L denotes the transmission distance over which the attenuation occurs, and α_{l_i} refers to the attenuation coefficient, which depends on the meteorological conditions. Several representative values of α_{l_i} under different weather situations are summarized in [16].

3.2 Atmospheric Turbulence

Atmospheric turbulence-induced fading is the result of variations in the refractive index of air caused by temperature and pressure inhomogeneities in the atmosphere. It induces variations in the received light intensity, thereby considerably impairing the efficacy of the free-space channel. The Rytov variance quantifies the turbulence strength, σ_R^2, which categorizes turbulence as weak, moderate, and strong for $\sigma_R^2 < 1$, $\sigma_R^2 \approx 1$, and $\sigma_R^2 > 1$, respectively. For planar wave propagation, the Rytov variance, represented as σ_R^2, is defined as [20] and can be expressed as

$$\sigma_R^2 = 2.25 k^{7/6} \sec^{11/6}(\psi) \int_{H_g}^{H_s} C_n^2(h_t) \left(h_t - H_g\right)^{5/6} dh_t, \tag{8}$$

where ψ is the zenith angle. $C_n^2(h_t)$ denotes the fluctuation of the refractive index structure parameter as articulated by the Hufnagel-Valley model [6, Eq. (19)] can be determined as

$$C_n^2(h_t) = 0.00594 \left(\frac{v_{\text{wind}}}{27}\right)^2 \left(10^{-5} h_t\right)^{10} \exp\left(-\frac{h_t}{1000}\right) + 2.7 \times 10^{-16} \exp\left(-\frac{h_t}{1500}\right) + C_n^2(0) \exp\left(-\frac{h_t}{100}\right), \tag{9}$$

where $C_n^2(0)$ is the ground level turbulence. v_{wind} (m/s) is the root mean squared wind speed, and its typical value of 21 m/s.

Various statistical distributions, such as log-normal distribution, Gamma-Gamma distribution, and Malaga distribution, have been analyzed in the literature to predict turbulence-induced fading with varying degrees of accuracy. This study utilizes the fading modeled by the Fisher-Snedecor $\mathcal{F}$ distribution, owing to its superior correlation with the empirical data. It is important to note that the Fisher-Snedecor $\mathcal{F}$ model offers a superior fit to experimental data for all turbulence conditions, while also providing more manageable mathematical expressions compared to the well-known Malaga $\mathcal{M}$ and Gamma-Gamma (GG) models. The probability distribution function (PDF) of the turbulence-induced fading coefficient h_t is written as [18]

$$f_{h_t}(h_t) = \frac{a^a (b-1)^b h_t^{a-1}}{\mathcal{B}(a,b)(a h_t + b - 1)^{a+b}}, \tag{10}$$

where $\mathcal{B}(\cdot)$ is the beta function [21]. The parameters a and b of the $\mathcal{F}$-distribution is given by [18]

$$a = \frac{1}{\exp\left(\sigma_{\ln \mathcal{S}}^2\right) - 1}, \tag{11}$$

and

$$b = \frac{1}{\exp\left(\sigma_{\ln \mathcal{L}}^2\right) - 1} + 2, \tag{12}$$

where $\sigma_{\ln \mathcal{S}}^2$ and $\sigma_{\ln \mathcal{L}}^2$ are the corresponding small-scale and large-scale log-irradiance variances can be found in [20]. In the following, (10) can be rewritten by supporting [22, Equation (8.4.2.5)]

$$f_{h_t}(h_t) = \frac{a^a h_t^{a-1}}{\mathcal{B}(a,b)(b-1)^a \Gamma(a+b)} \times G_{1,1}^{1,1}\left(\frac{a}{b-1} h_t \,\middle|\, \begin{matrix} 1-a-b \\ 0 \end{matrix}\right), \tag{13}$$

where $G_{p,q}^{m,n}(\cdot)$ is the Meijer-G function [21]. To obtain the cumulative distribution function (CDF) of the h_t, [23, Equation (26)] and [21, Equation (9.31.5)] are used together with some algebraic manipulations; the closed-form of CDF can be written as

$$F_{h_t}(h_t) = \frac{1}{\mathcal{B}(a,b)\Gamma(a+b)} G_{2,2}^{1,2}\left(\frac{a}{b-1} h_t \,\middle|\, \begin{matrix} 1-b & 1 \\ a & 0 \end{matrix}\right). \tag{14}$$

3.3 Misalignment-Induced Fading

The pointing error is due to the misalignment of the beam between the transmitter and receiver. Mechanical jitter between the OIRS and the receiver can cause the light spot to fluctuate at random within a specific range. According to the physical model of the OIRS jitter, the probability density function of the jitter angle at the receiving plane can be expressed as [10]

$$f_{\theta_{u_i}}(\theta_{u_i}) = \frac{\theta_{u_i}}{\left(1 + L_{R_i}\right)^2 \sigma_{\theta_{u_i}}^2 + 4\sigma_\phi^2} e^{\frac{-\theta_{u_i}^2}{2\left(1+L_{R_i}\right)^2 \sigma_{\theta_{u_i}}^2 + 8\sigma_\phi^2}}, \tag{15}$$

where $L_{R_i} = L_{s_i o_i} / L_{o_i u_i}$ represents the ratio of the distance from the source of the i-th region, $L_{s_i o_i}$, to the OIRS region of the i-th, and the distance from the OIRS region of the i-th to the receiver of the i-th, $L_{o_i u_i}$.

Table I
Comparative table of the turbulence-induced fading model

Characteristics	**Log – normal**	**Gamma – Gamma**	$\alpha - \mu$	**Malaga**	**Fisher-Snedecor**
Advantages	Easy to understand; simple model	Accurately describes both weak and strong turbulence	Flexible, capable of representing multiple fading conditions	Most general model, encompassing several other distributions	Closed-form expression, mathematically tractable
Disadvantages	Inaccurate under strong turbulence	Complex for performance analysis	Difficult to estimate parameters $alpha$ and μ from experimental data	Highly complex expressions, often lack closed-form solutions	Less physically intuitive than Gamma –Gamma
Apply for	Simple theoretical analysis	Practical channel simulation	Generalized fading modeling in RF and FSO	Complex experimental modeling, advanced 6G/FSO systems	Simplified statistical analysis compared to Málaga
Computational complexity	Low	Moderate	Moderate	High	Low–to– moderate
Experimental fitting	Poor fit under strong turbulence [17]	Fairly good fit [18]	Fit varies depending on conditions [19]	Good fit [18]	Good fit

Let $\theta \sim \mathcal{N}(0, \sigma_\theta^2)$ represent the pointing error angle at the transmitter, and $\phi \sim \mathcal{N}(0, \sigma_\phi^2)$ denote the deflection angle at the OIRS. The instantaneous displacement from the receiver center to the receiving light spot can be computed as the angle θ_{u_i}, which corresponds to the optical beam offset in the receiver plane r_i, which can be expressed as

$$r_i = \tan(\theta_{u_i}) L_{o_i u_i} \approx \theta_{u_i} L_{o_i u_i}. \tag{16}$$

The pointing error h_{p_i} owing to the vibrations of HAP, where OIRS is located, can be given as

$$h_{p_i} = A_0 \exp\left(-\frac{2r_i^2}{w_{Leq}^2}\right), \tag{17}$$

where $A_0 = [\mathrm{erf}(v)]^2$ is the fraction of the collected power at $r_i = 0$ and $w_{Leq}^2 = w_L^2 \frac{\sqrt{\pi}\mathrm{erf}(v)}{2v\exp(-v^2)}$ is the equivalent beam width in which $v = \sqrt{\frac{\pi}{2}}\frac{a}{w_L}$ is the ratio between aperture radius and the beam width and $w_L = (2\lambda)/(\pi\theta_T)$ is the beam waist radius in which θ_T is the divergence angle.

By substituting (16), (17) into (15) and applying some manipulations, the PDF of h_{p_i} can be given as

$$f_{h_{p_i}}(h_{p_i}) = \frac{w_{Leq}^2}{4A_0\left(\sigma_\theta^2 L_{T,i}^2 + 4\sigma_\beta^2 L_{s_i o_i}^2\right)}\left(\frac{h_{p_i}}{A_0}\right)^{\frac{w_{Leq}^2}{4\sigma_\theta^2 L_{T,i}^2 + 16\sigma_\beta^2 L_{s_i o_i}^2}}. \tag{18}$$

3.4 Composite Channel

The Fischer-Sensecor $\mathcal{F}$ distribution is used to model the fading caused by weak turbulence. From (7), (13), and (18), we can get the PDF of the channel coefficient as

$$\begin{aligned} f_{h_i}(h_i) &= \int_0^\infty \frac{1}{h_{l_i} h_{t_i}} f_{h_{p_i}}\left(\frac{h_i}{h_{l_i} h_{t_i}}\right) f_{h_{t_i}}(h_{t_i})\, dh_{t_i} \\ &= \frac{a^a}{\mathcal{B}(a,b)(b-1)^a \Gamma(a+b)} \frac{\xi^2}{A_0^{\xi^2}} \\ &\times \int_0^\infty \frac{1}{h_{l_i} h_{t_i}}\left(\frac{h_i}{h_{l_i} h_{t_i}}\right)^{\xi^2} h_{t_i}^{a-1} G_{1,1}^{1,1}\left(\frac{a}{b-1} h_{t_i} \middle| \begin{matrix} 1-a-b \\ 0 \end{matrix}\right) dh_{t_i}, \end{aligned} \tag{19}$$

where $\xi^2 = \frac{w_{Leq}^2}{4\sigma_\theta^2 L_{T,i}^2 + 16\sigma_\beta^2 L_{s_i o_i}^2}$. In addition, $\Gamma(\cdot)$ is the complementary error function [24].

By using a mathematical methodology approach in [25] and [23, Equation (24)], the closed-form expression of Equation (19) can be derived as

$$\begin{aligned} f_{h_i}(h_i) &= \frac{a\xi^2}{(b-1) A_0 h_l \Gamma(a)\Gamma(b)} \\ &\times G_{2,2}^{2,1}\left[\frac{a}{(b-1)A_0 h_l} h \middle| \begin{matrix} -b & \xi^2 \\ a-1 & \xi^2 - 1 \end{matrix}\right]. \end{aligned} \tag{20}$$

The precision of the PDF channel coefficient, h_i, is corroborated through the application of a Monte Carlo simulation utilizing a discrete-event simulator, as depicted in Figure 3. To do this, 10^6 independent samples are produced with the Senedecor-Fisher $\mathcal{F}$ model as specified in (13). Furthermore, assuming a specified OIRS jitter variance, $\sigma_{\theta_{u_i}}^2$, which can be derived from σ_θ^2 and σ_ϕ^2, we produce 10^6 random variables of h_{p_i} according to (17). Subsequently, a deterministic propagation loss coefficient, h_l, of 10^6 is produced using Equation (7). In this case, we investigate three situations with the different divergence angles, θ_T, of 3 mrad,

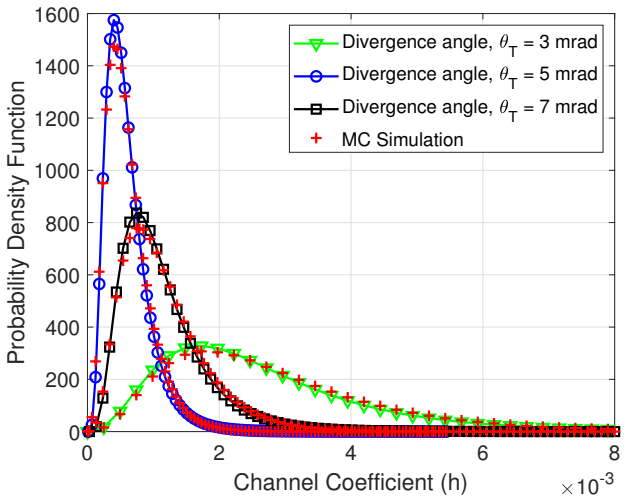

Figure 3. The PDF of the fading channel coefficient, h_i, verified by the Monte-Carlo simulations for different divergence angle, θ_T.

5 mrad, and 7 mrad to validate the accuracy of the theoretical model.

4 Performance Analysis

4.1 Signal-to-Noise Ratio (SNR)

Given the fact that the regions within the OIRS are contiguous and the area of each OIRS region is typically small, each region will probably intercept signals from various sources. Nonetheless, OIRS lacks signal processing capabilities, making it unable to discern the origin of the signals. As a result, it indiscriminately reflects all intercepted signals to the user; hence, the interference contribution from $\sum_{j=1,j\neq i}^{n} h_{s_j,o_i} h_{o_i,u_i} s_j$ is dominant compared to other interference signals. Therefore, the instantaneous SNR of user i γ_i can be determined as

$$\gamma_i = \frac{2h_i^2 P_i^2 \Re^2}{2\sum\limits_{j=1,j\neq i}^{N} h_i^2 P_j^2 \Re^2 + \sigma_{g_i}^2}, \tag{21}$$

where P_j is the transmit power from other sources reflected to the i-th user. $\Re$ is the responsivity of the photodetector and $\sigma_{g_i}^2$ is the variance of receiver noise. By using the variable transformation method and the average over the fading channel created in Equation (20), the PDF of the instantaneous SNR of the ith user is given as in Equation (22).

4.2 Outage Probability (OP)

The outage probability represents the probability that the instantaneous SNR falls below a predetermined outage threshold, γ_{th}. In our study, the user's outage probability can be derived as

$$P_{out}(\gamma_{th}) = \Pr[\gamma_i \leq \gamma_{th}] = \int_0^{\gamma_{th}} f_{\gamma_i}(\gamma_i)\, d\gamma_i$$

$$P_{out}(\gamma_{th}) = \int_0^{\gamma_{th}} \frac{P_t^2 \xi^2 \sigma_n^2 a}{(b-1) A_0 h_l \Gamma(a) \Gamma(b) \mathcal{T}} \times G_{2,2}^{2,1}\left[\frac{a}{(b-1) A_0 h_l} \mathcal{T} \middle| \begin{matrix} -b & \xi^2 \\ a-1 & \xi^2 - 1 \end{matrix} \right] d\gamma_i \tag{23}$$

where $\mathcal{T} = \sqrt{\gamma_i \sigma_n^2 \left(2P_t^2 - 2\sum\limits_{j=1,j\neq i}^{N} P_j^2 \gamma_i \right)^3}$

4.3 Correlation Coefficient

Correlation among sub-channels is sometimes unavoidable in actual FSO systems, especially when the link is long and/or the aperture separation is modest. This negative effect significantly diminishes the spatial diversity gain. As a result, channel correlation prediction is critical in assessing overall system performance. In our considered system, it is necessary to estimate the distance between adjacent OIRS elements to reduce optical crosstalk and increase the diversity gain. The correlation coefficient can be calculated as a function of the turbulence strength, link range, RIS size, and aperture spacing between two OIRS elements separated by the propagation distance. $\zeta(\Delta d)$ denotes the spatial covariance function, which is defined as

$$\zeta(\Delta d) = \exp\left\{ 8\pi^2 k^2 L \int_0^1 \int_0^\infty \kappa \phi_{n,\text{eff}}(\kappa)\, J_0(\kappa \Delta d) \times \exp\left(\frac{-d_i^2 \kappa^2}{16} \right) \left[1 - \cos\left(\frac{L\kappa^2 \xi}{k} \right) \right] d\kappa d\xi \right\} - 1, \tag{24}$$

where $J_0(\cdot)$ is the Bessel function of the first kind and of zero order, and $\phi_{n,eff}(\kappa)$ represents the effective atmospheric spectrum. κ and ξ can be found in [26]. Assuming the case of the zero-inner scale and the infinity-outer scale, $\phi_{n,eff}(\kappa)$ is given by

$$\phi_{n,\text{eff}}(\kappa) = 0.033 C_n^2 \kappa^{-\frac{11}{3}} \left[\exp\left(\frac{-\kappa^2}{\kappa_{X,0}^2} \right) + \frac{\kappa^{\frac{11}{3}}}{\left(\kappa^2 + \kappa_{Y,0}^2 \right)^{\frac{11}{6}}} \right], \tag{25}$$

where $\kappa_{X,0}^2 = \frac{k}{L} \frac{2.61}{1+1.11\sigma_R^2}$, $\kappa_{Y,0}^2 = \frac{3k}{L} \left(1 + 0.69\sigma_R^{12/5} \right)$.

5 Numerical Results and Discussions

This section presents the numerical results obtained based on the mathematical expressions derived in the previous section. We evaluated performance metrics in varying settings, including alterations in the partition of the array inside the OIRS, fluctuations in transmission distance, and modifications in environmental factors, particularly atmospheric turbulence. The fixed system parameters include an laser wavelength of 1550 nm and a σ_g of 10^{-7} (A/Hz). The distance from the source to

$$f_{\gamma_i}(\gamma_i) = \frac{P_t^2 \xi^2 \sigma_n^2 a}{(b-1) A_0 h_l \Gamma(a) \Gamma(b) \sqrt{\gamma_i \sigma_n^2 \left(2P_t^2 - 2 \sum_{j=1, j\neq i}^{N} P_j^2 \gamma_i\right)^3}} \times G_{2,2}^{2,1}\left[\frac{a}{(b-1) A_0 h_l} \sqrt{\frac{\gamma_i \sigma_n^2}{2P_t^2 - 2 \sum_{j=1, j\neq i}^{N} P_j^2 \gamma_i}} \middle| \begin{matrix} -b & \xi^2 \\ a-1 & \xi^2 - 1 \end{matrix}\right] \quad (22)$$

the OIRS and from the OIRS to the users is 20 km. The aperture radius is 10 cm, OIRS size is 1 m, and the signal-to-noise ratio threshold, γ_{th}, is -5 dB.

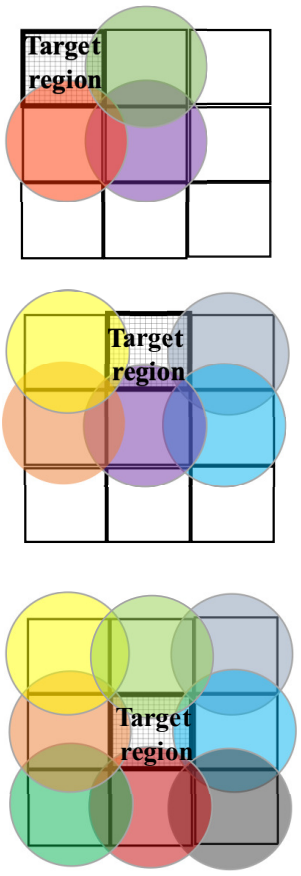

Figure 4. The illustration of the crosstalk optical power impacts on the different OIRS element positions.

First, we investigate the relationship between the outage probability of the system and the zenith angle under different interference sources on the OIRS as shown in Figure 5. In addition, we consider two scenarios with different divergence angles, θ_T, to comprehensively evaluate the system performance. How targeted users are affected by different number of interference sources is clarified by using Figure 4, which is shown the relative positions of the targeted users. When the optical beam of the considered user reaches the OIRS at the **corner**, it is affected by three interference sources before it is reflected. If the reflected beam emerges at the **edge** of the OIRS, the targeted user is affected by

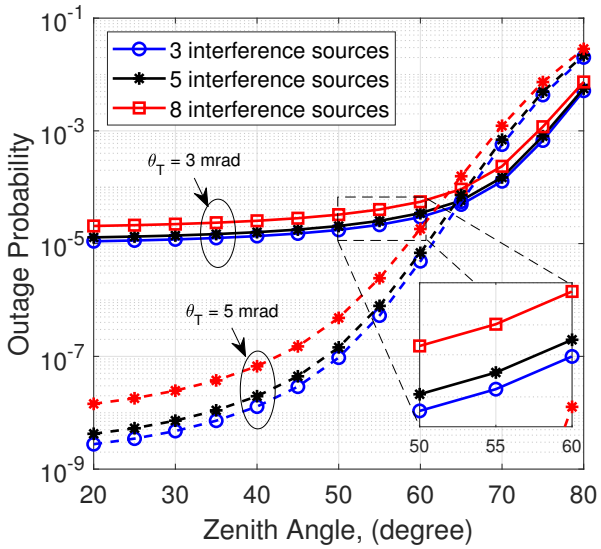

Figure 5. Outage performance versus zenith angle in different conditions from the optical crosstalk with the transmitted power of 25 dBm.

five interference sources, causing performance degradation. Finally, if the optical beam is reflected at the **center** of the OIRS, it interferes with eight other sources around it. This case causes the highest value of outage probability, while the lowest one is when the beam is reflected at the corner of OIRS.

In addition, the zenith angle is directly related to the influence of atmospheric turbulence on signal quality. The higher the zenith angle, the stronger the turbulent strength [6]. Looking at the results, we can see that, in the case of zenith angle from 20 to 65 degrees (corresponding to the weak to moderate turbulence regime), the effect of the interference optical power becomes more obvious, especially in the case of divergence angle equal to 3 mrad, i.e., the turbulent strength varies but the performance is almost unchanged. In contrast, from 65 to 80 degrees (moderate to strong turbulence regime), atmospheric turbulence shows a significant impact as the outage probability increases rapidly.

Next, Figure 6 focuses on exploring the effect of turbulence on the outage performance over the transmitted power range of 15 to 35 dBm. In this result, we consider 8 interference sources, a divergence angle of 5 mrad, and a zenith angle of 60 degrees. Clearly, the outage probability is relaxed in weak to moderate turbulence regimes, i.e., $C_n^2(0) = 5 \times 10^{-15}$

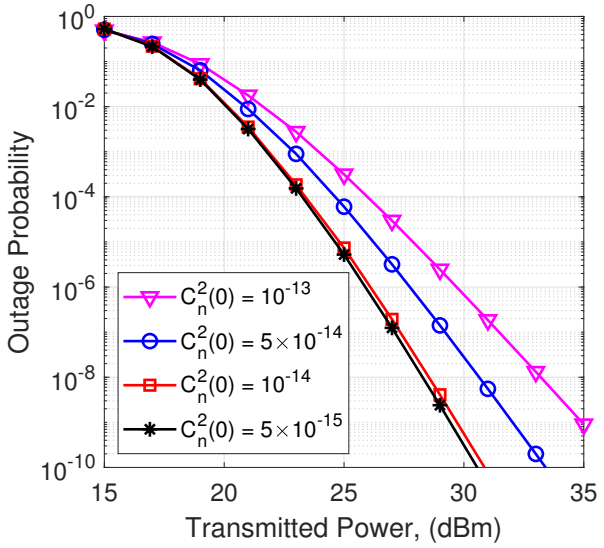

Figure 6. Outage performance versus transmitted power with different atmospheric turbulence conditions.

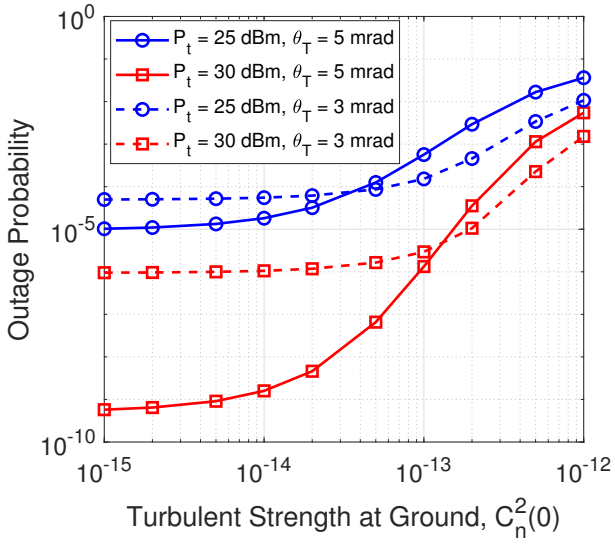

Figure 8. Outage performance versus turbulent strength.

and $C_n^2(0) = 10^{-14}$. However, it becomes stronger in the case of strong turbulence as a result of the greater fluctuation of optical power intensity. More specifically, the system must compensate for 4 dB of power in the case of strong turbulence to maintain the outage probability of 10^{-6} as compared to weak turbulence.

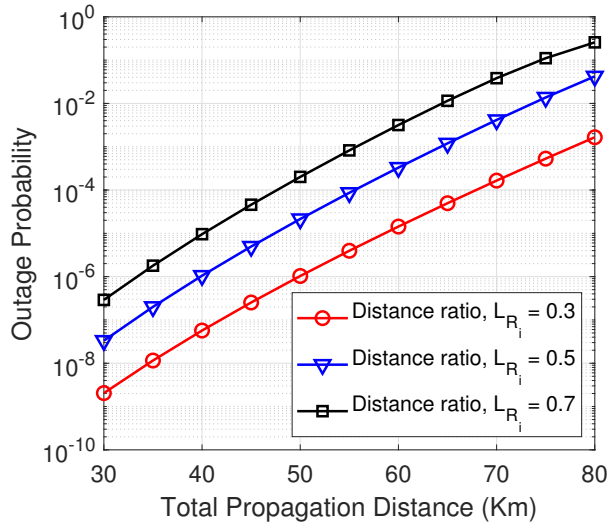

Figure 7. Outage probability versus total transmission distance

Figure 7 presents the outage performance of the OIRS-assisted multiuser FSO system on HAP and investigates over the range of total transmission distance, denoted as L, from 30 km to 80 km with different distance ratios ($L_{R_i} = 0.3, 0.5, 0.7$). The distance ratio is defined as $L_{R_i} = \frac{L_{s_i,o_i}}{L_{oi,ui}}$, where L_{s_i,o_i} is the distance from the base station (source) to the i-th OIRS region, and L_{o_i,u_i} is the distance from the i-th OIRS region to the i-th user (total $L = L_{s_i,o_i} + L_{o_i,u_i}$). In this case, the parameters are set up by utilizing the transmit power $P_t = 25$ dBm, beam divergence angle $\theta_T = 3$ mrad, moderate atmospheric turbulence ($C_n^2 = 10 \times 10^{-14}$ using the Fisher-Snedecor $\mathcal{F}$ channel model), and 8 interference sources. Outage probability rises sharply with L due to accumulated path loss and turbulence-induced fading, aligning with the $\mathcal{F}$-Snedecor distribution's tail behavior (superior to Gamma-Gamma for moderate/strong turbulence, as benchmarked in Table I). Increasing L_{R_i} curbs crosstalk-induced outages (lowering interference terms in Equation 3c–3d) but heightens fading accumulation, driving higher probabilities in extended links. For example, $L_{R_i} = 0.3$ positions the OIRS closer to the source (occupying 30% of the total distance), which helps reduce propagation loss in the OIRS-to-user leg but may increase crosstalk due to narrower beams at shorter distances.

For a comprehensive performance analysis, the impact of atmospheric turbulence on multiuser FSO systems is shown in Figure 8, where the outage probability is evaluated over a range from weak to strong atmospheric turbulence. The result is obtained for the case of eight interference sources; two values of transmitted powers, 25 and 30 dBm, and two values of the divergence angle, 3 and 5 mrad. In the case of setting a small divergence angle, the beam is less spread and the received power is better. Consequently, the effect of atmospheric turbulence is mitigated, resulting in a lower probability of outage. In contrast, a higher outage probability is seen due to lower received power obtained in the case of a divergence angle of 5 mrad.

As discussed above, the influence of the optical crosstalk is significant, especially when the density of OIRS elements is high, especially in the case of the optical beam is reflected at the center of OIRS. Therefore, to mitigate this influence, we try to design an OIRS, whose elements are spaced apart to reduce optical crosstalk as shown in Figure 9. In fact, the OIRS elements are nearby on the same receiving plane; it can be inferred that the turbulence parameters and propagation loss for their

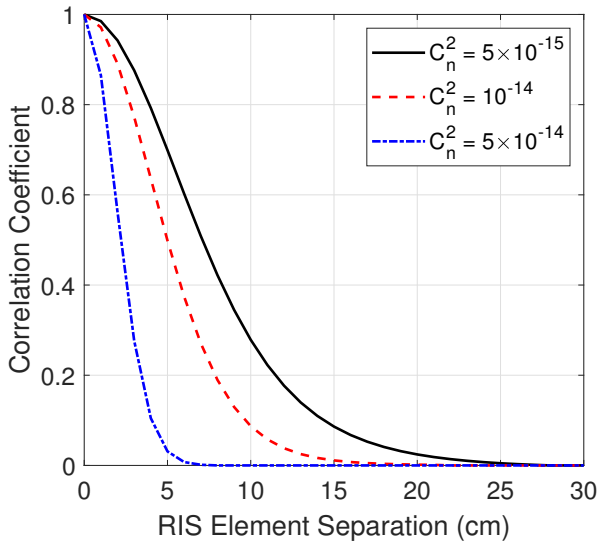

Figure 9. RIS element separation design for reducing crosstalk optical power by considering correlation coefficient with different values of turbulence strength.

respective channels remain consistent over transmission distance. Hence, the distance between the RIS elements must be sufficient to prevent any correlation or reliance caused by turbulence-induced fading. The paper [26] reported a connection between the channel correlation coefficient and the distance between the detection points. Referencing [26, Equation (4)], we can determine that in order to achieve channel independence for the indicated weak, moderate, and high turbulence conditions, separation distances of at least 7 cm, 15 cm, and 25 cm are required, respectively.

6 Conclusion

This study has comprehensively evaluated the performance of an OIRS-assisted HAP-based FSO system under the influence of optical crosstalk and atmospheric turbulence. By equipping OIRS on HAP, the proposed system can enhance connectivity abilities, i.e., supporting multiple users and overcoming the obstacles or LoS requirement. The analysis focused on outage probability, considering critical factors such as atmospheric turbulence, propagation loss, and pointing misalignment. Numerical results demonstrated that the system's performance is significantly affected by optical crosstalk, especially when the density of OIRS elements is high. For designing an OIRS that effectively reduces optical crosstalk and enhances channel independence, we find that element separation should be at least 7 cm, 15 cm, and 25 cm for weak, moderate, and strong turbulence conditions, respectively. These findings highlight the importance of the OIRS design in minimizing interference and improving the reliability of the system.

Future research directions include exploring advanced OIRS configurations to further minimize crosstalk optical power, such as adaptive beamforming techniques or dynamic element allocation. Additionally, incorporating machine learning algorithms to predict and compensate for atmospheric turbulence effects could enhance system performance. Investigating the integration of OIRS-aided FSO systems with hybrid RF/FSO networks or quantum communication protocols may also provide new opportunities for robust, high-capacity communication systems in next-generation networks.

Acknowledgment

This research is funded by Vietnam National Foundation for Science and Technology Development (NAFOSTED) under grant number 102.02-2023.18.

References

[1] F. Tarhouni, R. Wang, and M.-S. Alouini, "Free Space Optical Mesh Networks: A Survey," *IEEE Open Journal of the Communications Society*, vol. 6, pp. 642–655, 2025.

[2] S. Prasad Tera, R. Chinthaginjala, G. Pau, and T. Hoon Kim, "Toward 6G: An Overview of the Next Generation of Intelligent Network Connectivity," *IEEE Access*, vol. 13, pp. 925–961, 2025.

[3] C.-W. Chow, "Recent Advances and Future Perspectives in Optical Wireless Communication, Free Space Optical Communication and Sensing for 6G," *Journal of Lightwave Technology*, vol. 42, no. 11, pp. 3972–3980, 2024.

[4] H.-B. Jeon, S.-M. Kim, H.-J. Moon, D.-H. Kwon, J.-W. Lee, J.-M. Chung, S.-K. Han, C.-B. Chae, and M.-S. Alouini, "Free-Space Optical Communications for 6G Wireless Networks: Challenges, Opportunities, and Prototype Validation," *IEEE Communications Magazine*, vol. 61, no. 4, pp. 116–121, 2023.

[5] T. V. M. Pham, T. V. Nguyen, N. T. T. Nguyen, T. A. Pham, H. T. T. Pham, and N. T. Dang, "Performance Analysis of Hybrid Fiber/FSO Backhaul Downlink over WDM-PON Impaired by Four-Wave Mixing," *Journal of Optical Communications*, vol. 41, no. 1, pp. 91–98, 2020. [Online]. Available: https://doi.org/10.1515/joc-2017-0127

[6] T. V. Nguyen, H. D. Le, N. T. Dang, and A. T. Pham, "On the Design of Rate Adaptation for Relay-Assisted Satellite Hybrid FSO/RF Systems," *IEEE Photonics Journal*, vol. 14, no. 1, pp. 1–11, Feb. 2022.

[7] H. D. Le, T. V. Nguyen, V. Mai, and A. T. Pham, "FSO-Based HAP-Assisted Multi-UAV Backhauling Over $\mathcal{F}$ Channels With Imperfect CSI," *IEEE Transactions on Vehicular Technology*, vol. 73, no. 12, pp. 19 597–19 612, 2024.

[8] T. V. Nguyen, H. D. Le, and A. T. Pham, "On the Design of RIS–UAV Relay-Assisted Hybrid FSO/RF Satellite–Aerial–Ground Integrated Network," *IEEE Transactions on Aerospace and Electronic Systems*, vol. 59, no. 2, pp. 757–771, 2023.

[9] H. Wang, Z. Zhang, B. Zhu, J. Dang, L. Wu, and Y. Zhang, "Approaches to Array-Type Optical IRSs: Schemes and Comparative Analysis," *Journal of Lightwave Technology*, vol. 40, no. 12, pp. 3576–3591, 2022.

[10] H. Wang, Z. Zhang, B. Zhu, J. Dang, L. Wu, L. Wang, K. Zhang, Y. Zhang, and G. Y. Li, "Performance Analysis of Multi-Branch Reconfigurable Intelligent Surfaces-Assisted Optical Wireless Communication System in Environment With Obstacles," *IEEE Transactions on Vehicular Technology*, vol. 70, no. 10, pp. 9986–10 001, 2021.

[11] P. D. Pham, C. K. P. Nguyen, H. D. Le, H. T. T. Pham, T. V. Nguyen, and N. T. Dang, "Optical Intelligent Reflecting Surface-Assisted Multiple Users over Turbulence Channels," in *Proceedings of the 2024 RIVF International*

Conference on Computing and Communication Technologies (RIVF), 2024, pp. 45–50.
[12] H. Jia, J. Zhong, M. N. Janardhanan, and G. Chen, "Ergodic Capacity Analysis for FSO Communications with UAV-Equipped IRS in the Presence of Pointing Error," in *Proceedings of the 2020 IEEE 20th International Conference on Communication Technology (ICCT)*, 2020, pp. 949–954.
[13] S. Malik, P. Saxena, and Y. H. Chung, "Performance analysis of a UAV-based IRS-assisted hybrid RF/FSO link with pointing and phase shift errors," *Journal of Optical Communications and Networking*, vol. 14, no. 4, pp. 303–315, Apr. 2022.
[14] P. Saxena and Y. H. Chung, "On the performance of all-optical RORIS dual hop UAV based FSO systems," *ICT Express*, vol. 9, no. 3, pp. 466–472, 2023.
[15] H. Ajam, M. Najafi, V. Jamali, B. Schmauss, and R. Schober, "Modeling and Design of IRS-Assisted Multi-link FSO Systems," *IEEE Transactions on Communications*, vol. 70, no. 5, pp. 3333–3349, 2022.
[16] T. V. Nguyen, H. T. Nguyen, H.-C. Le, N. D. Nguyen, and N. T. Dang, "Performance analysis of gigabit-capable mobile backhaul networks exploiting TWDM-PON and FSO technologies," in *Proceedings of the 2016 International Conference on Advanced Technologies for Communications (ATC)*, 2016, pp. 180–185.
[17] M. Atiyah, L. Abdulameer, and G. Narkhedel, "PDF Comparison based on Various FSO Channel Models under Different Atmospheric Turbulence," *Al-Khwarizmi Engineering Journal*, vol. 19, pp. 78–89, 12 2023.
[18] K. P. Peppas, G. C. Alexandropoulos, E. D. Xenos, and A. Maras, "The Fischer-Snedecor $\mathcal{F}$-Distribution Model for Turbulence-Induced Fading in Free-Space Optical Systems," *Journal of Lightwave Technology*, vol. 38, no. 6, pp. 1286–1295, Dec. 2020.
[19] P. H. Almeida, L. R. Andrade, H. S. Silva, U. S. Dias, O. S. Badarneh, and R. A. de Souza, "The α-F composite distribution with pointing errors: Theory and applications to RIS," *Journal of the Franklin Institute*, vol. 361, no. 10, p. 106872, 2024.
[20] L. C. Andrews and R. L. Phillips, *Laser Beam Propagation through Random Media*, 2nd ed. Bellingham, WA: SPIE Press, 2005.
[21] I. S. Gradshteyn and I. M. Ryzhik, *Table of Integrals, Series, and Products, 7th Edition*. New York: Academic, 2007.
[22] A. Prudnikov, Y. Brychkov, and O. Marichev, *Integrals, and seriers: volume 3 more special function*. Gordon and Breach Science Publishers, 1986, vol. 3.
[23] V. Adamchik and O. Marichev, "The algorithm for calculating integrals of hyperfeometric type functions and its realization in reduce system," *Proceedings of the International Symposium on Symbolic and Algebraic Computation*, pp. 212–224, 1990.
[24] A. Prudnikov, Y. Brychkov, and O. Marichev, *Integrals and Series. Volume 3: More Special Functions*, 10 1989.
[25] O. S. Badarneh, R. Derbas, F. S. Almehmadi, F. El Bouanani, and S. Muhaidat, "Performance Analysis of FSO Communications Over F Turbulence Channels With Pointing Errors," *IEEE Communications Letters*, vol. 25, no. 3, pp. 926–930, 2021.
[26] P. V. Trinh, T. V. Pham, and A. T. Pham, "Free-Space Optical Systems over Correlated Atmospheric Fading Channels: Spatial Diversity or Multihop Relaying?" *IEICE Transactions on Communications*, vol. E101.B, no. 9, pp. 2033–2046, 2018.

Bach Q. Tran received B.E. from HCMC University of Technology and Education (HCMUTE), Vietnam, in 2007. He obtained M.E. degrees in Electronic Engineering from Military Technical Academy (MTA), Vietnam in 2013, respectively. Now, he is a lecturer at University of Economics - Technology for Industries (UNETI) in Faculty of Electronics and Computer Engineering. His current research interests are design and performance analysis of FSO systems and intelligent reflecting surfaces.

Thang V. Nguyen received a B.E. degree in Electronics and Telecommunications Engineering from the Posts and Telecommunications Institute of Technology (PTIT) of Vietnam in 2017, and the M.E. and Ph.D. degrees in Computer Science and Engineering from the University of Aizu (UoA), Japan, in 2019 and 2022, respectively. He is a lecturer at the Posts and Telecommunications Institute of Technology. He was also an invited/visiting researcher at the Computer Communications Lab. the University of Aizu, Japan, in 2023. His current research interests include network modeling and performance analysis, particularly on space-air-ground integrated networks, optical wireless communications, quantum key distribution, hybrid FSO/RF systems, and intelligent reflecting surfaces. He won the IEEE ICCE Best Paper Award in 2022 and the Springer ICISN Best Paper Award in 2025.

Hien T. T. Pham received the B.E. Degree from Hanoi University of Transport and Communications in 1999; and the M.E. and Ph.D. degrees in Telecommunication Engineering from Posts and Telecommunications Institute of Technology (PTIT) in 2005 and 2017, respectively. She has been working at the Department of Wireless Communications of PTIT since 1999. Dr. Pham is currently a senior lecturer at PTIT. Her present research interests are in the area of design and performance evaluation of optical and wireless communication systems. She won the IEEE ISCIT Best Paper Award in 2019 and the Springer ICISN Best Paper Award in 2025.

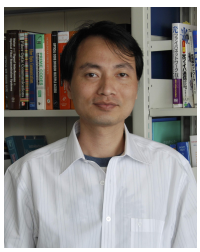

Ngoc T. Dang received the B.E. degree from the Hanoi University of Technology, Hanoi, Vietnam in 1999, and the M.E. degree from the Posts and Telecommunications Institute of Technology (PTIT), Hanoi, Vietnam in 2005, both in electronics and telecommunications; and received the Ph.D. degree in computer science and engineering from the University of Aizu, Aizuwakamatsu, Japan in 2010. He is currently an Associate Professor/Head with the Department of Wireless Communications at PTIT. He was also an invited/visiting researcher at FOTON ENSSAT Lab., Universite de Rennes 1, France, in 2011 and Computer Communications Lab., The University of Aizu, Japan in 2012, 2013, 2015, and 2017. His current research interests include the area of communication theory with a particular emphasis on modeling, design, and performance evaluation of optical CDMA, RoF, optical wireless communication and quantum key distribution systems. He won the IEEE ISCIT Best Paper Award in 2019, the IEEE RIVF Best Paper Award in 2023, and the Springer ICISN Best Paper Award in 2025. He is a senior member of IEEE.